THE GROWTH OF A ROTARY GRAVITY WAVE IN A CYLINDRICAL CONTAINER

H. Steinrück, A. Maly

Abstract: In phase condenser mode the water level in the draft tube of a Francis turbine is lowered, and thus, the runner of the turbine rotates in the air. The rotary motion of the rotor may induce a rotary surface wave with a large amplitude. In this study, a simplified setup will be investigated. We consider a vertical cylindrical container with a rotating disc at its top end. In this paper, an asymptotic stability analysis with respect to suitable dimensionless parameters of the axis-symmetric water flow will be performed. Moreover, the temporal evolution of the rotary wave will be studied experimentally.

1 Introduction

In phase condenser mode the water level in the draft tube of a Francis turbine is lowered, and the runner runs in air dissipating electrical energy. The rotary motion of the runner may induce a rotary wave of large amplitude in the water, see Ceravola et al. [2], Tanaka et al. [13], and Vagnoni et al. [14].

In this paper, we will describe the mechanism which excites the wave. For this purpose we will investigate a simplified flow configuration: We consider a vertical cylinder of radius $\tilde{R}$ and height $\tilde{H}$, partially filled with water. At rest state, the water depth is $\tilde{h}_W$. The top lid of the cylinder rotates with an angular speed $\tilde{\Omega}_A$ in its plane around the cylinder axis and sets the air above the water into a rotary motion.

To enhance the rotary air motion T-shaped profiles may be mounted on the top lid, see Fig. 1a. The wave form resembles very much the well-known potential wave shown in Fig. 1b.

The rotary air flow induces shear stress on the water surface which in turn will drive a flow in the water. For moderate rotation velocities of the lid, the air flow and the water flow are axis-symmetric. It has been observed, that this axis-symmetric flow will become unstable and rotary waves will form if the angular speed of the lid is increased above a certain threshold.

Nowadays, one may think that the method of choice would be a CFD simulation of the whole system including both phases. However, due to the large Reynolds numbers and that it takes several thousands of revolutions of the disc (rotor) until the wave forms asymptotic methods to study the instability mechanism seem to be more appropriate. Shear stress-induced water waves have been studied by many authors in the context of ocean waves. Miles [7] described an instability mechanism based on the interaction

of the shear flow of air above a water surface. Among other authors Sajjadi [8] the ideas of Miles to the growth of weakly non-linear Stokes waves. The excitation mechanism of Miles and Sajjadi requires that there is no base flow in the water.

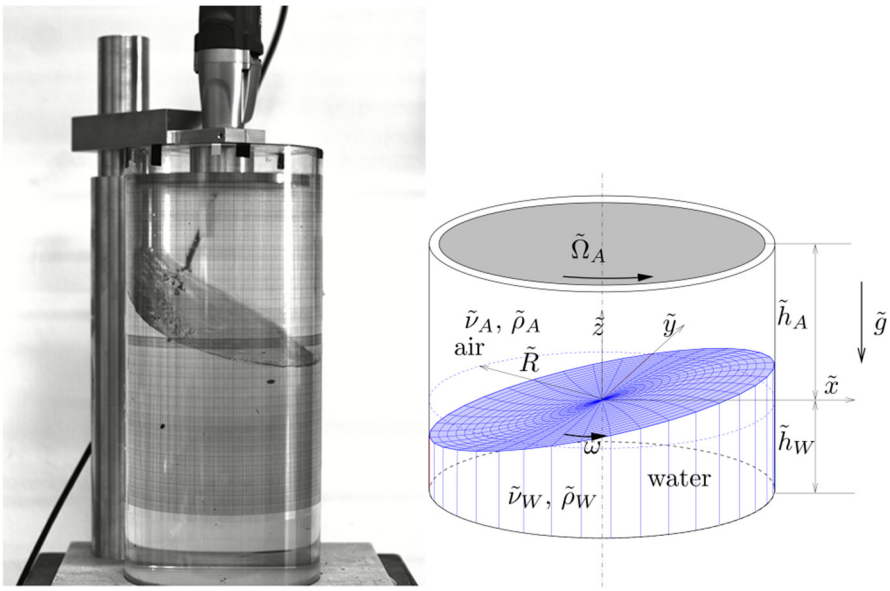

a) b)

Fig. 1. Experimental setup a). Inviscid rotary wave with one crest b)

Bye and Ghantous [1], [5] investigated waves in a circular container induced by a rotating air flow by an inviscid Kelvin-Helmholtz mechanism.

Here, we will follow a different approach. We investigate the stability of the axis-symmetric base flow induced by the air flow by an asymptotic expansion with respect to suitable parameters, for large Reynolds number of the wave and small Ekman numbers of the base flow. In that setting, it turns out that the pressure response of the air flow to surface undulations does not influence the leading order terms of the stability analysis, cf. Steinrueck and Maly [11],[12].

Since the dynamic viscosity of air is much smaller than that of water, we can decouple the two-phase flow problem into two single-phase flow problems. We assume that the slow water flow will not influence the air flow above as long as the wave amplitudes are small. Thus, the water faces an almost unchanged axis-symmetric shear stress distribution and pressure distribution on its surface.

We will begin our analysis by dimensional analysis, then describe the inviscid wave mode. The core of the paper will be a stability analysis of the axis-symmetric base flow in the limit of large Reynolds numbers. Finally, we report some experimental observations.

symbol	Reference value	comment
h_W	$\tilde{R}$	Water depth at rest
h_A	$\tilde{R}$	Width of air gap
τ_θ	$\tilde{\tau}_0$	Azimuthal shear stress
τ_r	$\tilde{\tau}_0$	Radial shear stress
u, v, w	$(\tilde{g}\,\tilde{R})^{1/2}$	Velocity components
U_B, V_B, W_B	$\widetilde{\Omega}_0 \tilde{R}$	Vel. comp. of base flow
ω	$(\tilde{g}/\tilde{R})^{1/2}$	Angular wave speed
g	$(\tilde{g}/\tilde{R})^{1/2}$	Growth rate
Ek		Ekman number (3)
Fr		Froude number (5)
Re		Wave Reynolds number (4)
Re_A		Reynolds number of air flow
μ		Zero of derivative of Bessel function J_n

Table 1: List of variables, dimensional variables are denoted by $\tilde{}$

2 Governing equations and Scaling

Since we are primarily interested in the excitation mechanism of the wave, we will investigate the stability of the axis-symmetric base state. We assume that the air flow is given and is not influenced by the flow in the water as long as the wave amplitude is much smaller than the cylinder radius. In the following dimensional quantities are denoted with a tilde, and thus, quantities without a tilde are dimensionless. We assume that the shear stress distributions at the free surface are given as

$$\tilde{\tau}_\theta = \tilde{\tau}_0 \tau_\theta(r), \quad \tilde{\tau}_r = \tilde{\tau}_0 \tau_r(r), \quad \tilde{\tau}_0 = 4 \int_0^{\tilde{R}} \tilde{\tau}_\theta \tilde{r}^2 \mathrm{d}\tilde{r} / \tilde{R}^2 \tag{1}$$

where $\tilde{\tau}_0$ is a suitable reference value for the surface shear stresses.
Assuming laminar flow in the water, we can estimate the angular velocity Ω_0 of the base flow. But before we introduce the Ekman number $Ek = \tilde{\nu}/\tilde{R}^2\widetilde{\Omega}_0$, where $\tilde{\nu}$ is the kinematic viscosity of the water. For small Ekman-numbers, we expect a boundary-layer of thickness $\tilde{R}\sqrt{Ek}$ near the free surface. Thus, we can estimate

$$\tilde{\tau}_0 = \frac{1}{\sqrt{Ek}} \tilde{\rho}\tilde{\nu}\tilde{\Omega}_0 = \tilde{\rho}\sqrt{\tilde{\nu}}\tilde{R}\tilde{\Omega}_0^{3/2}, \tag{2}$$

and express $\widetilde{\Omega}_0$ in terms of the reference value of the surface shear stress. We obtain

$$\tilde{\Omega}_0 = \left(\frac{\tilde{\tau}_0^2}{\tilde{\rho}^2\tilde{\nu}\tilde{R}^2}\right)^{1/3}, \quad Ek = \left(\frac{\tilde{\rho}}{\tilde{\tau}_0}\frac{\tilde{\nu}^2}{\tilde{R}^2}\right)^{2/3}. \tag{3}$$

A reference value for the angular wave speed can be found by assuming that the wave is almost inviscid and that the water is deep $h_W = \tilde{h}_W/\tilde{R} \gg 1$. Thus, the angular wave speed can only depend on the gravity acceleration $\tilde{g}$, the container radius $\tilde{R}$ and the density of the fluid $\tilde{\rho}$. Using this data, the reference angular velocity has to be $\sqrt{\tilde{g}\tilde{R}}$. Thus, the ratio between inertia and viscous forces of the wave is characterized by the wave Reynolds number

$$Re = \tilde{R}^2\sqrt{\tilde{g}/\tilde{R}}/\tilde{\nu}. \tag{4}$$

The ratio between the characteristic angular speed of the base flow and the characteristic angular wave speed can be interpreted as a Froude number.

$$Fr = \frac{\tilde{\Omega}_0}{\sqrt{\tilde{g}/\sqrt{R}}} = \frac{1}{Re\,Ek}. \tag{5}$$

The governing equations for the fluid motion are the Navier-Stokes equations. We choose a cylindrical coordinate system with its origin on the cylinder axis at the free unperturbed water surface. We refer all lengths to the cylinder radius $\tilde{R}$. A natural choice for the timescale is the reciprocal value of the reference value for the angular wave speed, $1/\sqrt{\widetilde{\omega}_0}$. Thus, we scale the flow velocities accordingly.

At the free surface $z = h(r, \theta, t)$, we have to prescribe dynamic boundary conditions in the azimuthal, the radial, and the vertical direction, and the kinematic boundary condition.

Assuming a small Froude number the surface curvature due to centrifugal forces can be neglected for the base flow. Moreover, for the stability the linearized version of the dynamic shear stress boundary conditions are sufficient. They read in dimensionless form

$$\tau_\theta(r)\frac{Fr}{\sqrt{Ek}} = v_z + \frac{1}{r}w_\theta, \tag{6}$$

$$\tau_r(r)\frac{Fr}{\sqrt{Ek}} = u_z + w_r. \tag{7}$$

The dynamic boundary condition in vertical direction reads

$$-p + h + \frac{2}{Re}w_z = 0, \tag{8}$$

where p is the reduced (hydro-static pressure subtracted) dimensionless pressure referred to $\tilde{\varrho}\tilde{R}^2\widetilde{\omega}_0^2$ and h is the dimensionless height of the free surface. Additionally, the kinematic boundary condition has to be satisfied at the free surface

$$w = h_t + uh_r + \frac{1}{r} vh_\theta. \tag{9}$$

The Navier-Stokes equations in cylinder coordinates can be found in Schlichting and Gersten [9].

3 The base flow

To determine the base flow in the water, we prescribe shear stress distributions $\tilde{\tau}_\vartheta$\t and $\tilde{\tau}_r$ for the azimuthal and radial shear stress components at the free surface, which are determined by a CFD-simulation of the air flow in a cylinder driven by rotating top lid while the cylinder wall and the bottom are at rest.
In this paper, we will consider two different cases.

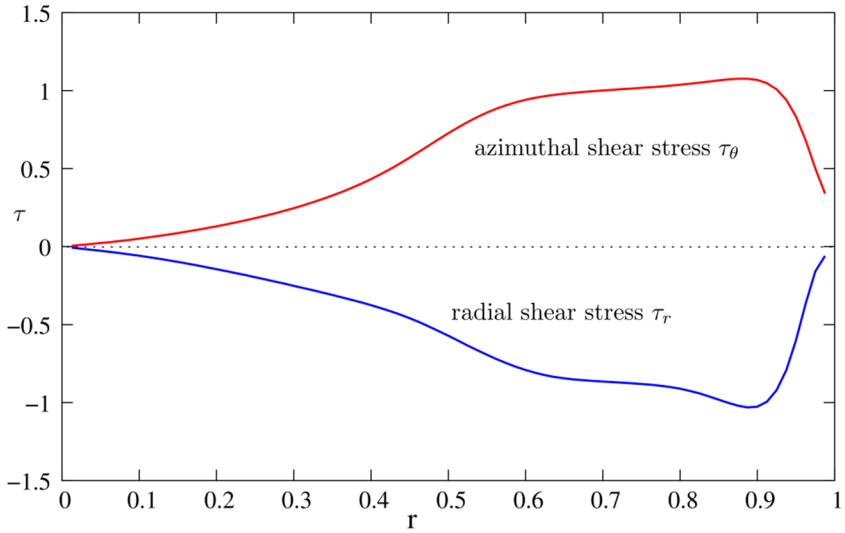

Fig. 2. Normalized bottom shear stress for case 2

- Case 1: laminar air flow $h_A = 2$, $Re_A = \tilde{R}^2\,\tilde{\Omega}_A\,/\tilde{\nu}_A = 10^3$. The normalized bottom shear stress distribution can approximated by

$$\tau_r = -0.75\,r\left(1 - e^{2.5(r-1)}\right)^3, \quad \tau_\theta = 0.25\,r(1-r) \quad .$$

- Case 2: turbulent air flow in a short cylinder $h_A = 0.125$, $Re_A = 3.07\ 10^5$. The air flow is computed using OpenFOAM employing the k,ω-SST turbulence model. The resulting normalized bottom shear stress distributions are shown in Fig. 2.

Assuming a small Froude number Fr, the free surface can be approximated by a horizontal plane, and we rescale the governing equations by

$$u = Fr\,U_B \quad v = Fr\,V_B, \quad w = Fr\,W_B. \tag{10}$$

Inserting this scaling into the Navier-Stokes equations, the Reynolds number is formally replaced by the reciprocal value of the Ekman number $1/Ek$.

Thus, for a given shear stress distribution the dimensionless flow field is determined by the dimensionless water depth h_W and the Ekman number Ek. Following Dijkstra et al. [3], the governing equations are reformulated in terms of a stream function ψ with $U_B = \psi_z/r$, $W_B = -\psi_r/r$ and the azimuthal velocity v. The resulting equations are discretized using a spectral method based on Chebychev polynomials.

Using up to $N = 80$ Chebychev-polynomials in r and z-direction, as well, we calculate the base flow for Ekman numbers in the interval 10^{-5} to 10^{-2} for both shear stress distributions. The solutions for $N = 40$ seem to be acceptable only for $Ek > 5\ 10^{-4}$ and agree well with the solutions for $N = 80$. We will give a short discussion on the accuracy of the solutions in the section 4.4 where we present the results for the growth rate.

In Fig. 3 the streamlines for case 2 for three values of the Ekman number are shown. We remark that the qualitative behaviour is similar to the flow in a cylinder with a rotating top lid. For $Ek = 5.62\ 10^{-4}$ a vortex breakdown at the centre line as described in Gelfgat [4] occurs. In the laminar flow case, the radial shear stress is larger than the azimuthal shear stress. As a consequence, the radial surface velocity is negative. Thus, at the free surface, there is a very thin layer of fluid flowing towards the axis. In the turbulent case, the azimuthal shear stress is larger than the radial shear stress component, and there is no inward directed fluid layer near the surface. Later, we will see that the flow behaviour near the surface influences the stability considerably.

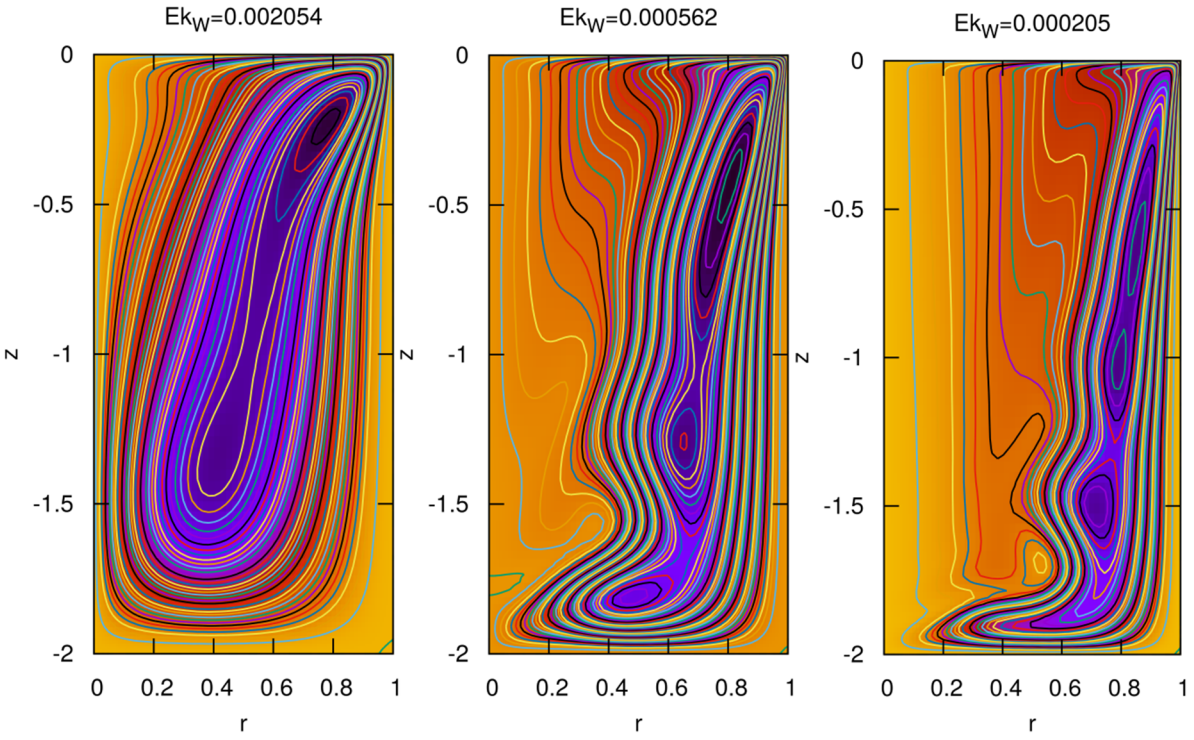

Fig. 3. Streamlines of the base flow for case 2 for different Ekman numbers

4 Asymptotic stability analysis

We want to investigate the stability of the base flow with respect to rotary waves. Thus, we linearize the governing equations around the base state and make the usual eigenvalue ansatz for the radial velocity component,

$$U = Fr\, U_B(r, z; Ek) + u(r, z, n\theta - \omega t)\exp^{gt} + \ldots \quad , \tag{11}$$

$$\omega = \omega_0 + \frac{1}{\sqrt{Re}}\omega_{1/2} + Fr\omega_1 + Fr^2\omega_2 + \ldots \quad , \tag{12}$$

$$g = \frac{1}{\sqrt{Re}}\omega_{1/2} + Fr^2 g_2 + \ldots \quad . \tag{13}$$

where ω/n is the angular wave speed and g the growth rate and n the wave number in the azimuthal direction. For the other velocity components and the pressure, we make a similar ansatz.

We expand the eigenfunction, angular velocity, and the growth rate with respect to large (wave) Reynolds numbers Re and small Froude numbers Fr. The Ekman number Ek has than the role of a coupling parameter and thus is small, too. In the interior, the flow field has an expansion of the form

$$u = u_0 + \frac{1}{\sqrt{Re}}u_{1/2} + Fr\, u_1 + Fr^2 u_2 + \ldots, \tag{14}$$

written here for the radial velocity component. We remark that a similar expansion is used for the angular wave speed and the growth rate. The expansion is primarily an expansion with respect to the Froude number Fr. This is indicated by the indices. Then the terms of the expansion are functions of the Ekman number Ek. We will evaluate the expansion terms under the assumption that the Ekman number $Ek \ll 1$ is small.

The zeroth-order term corresponds to an inviscid potential flow wave discussed in the following subsection and well known from sloshing. However, at the solid surfaces, the inviscid approximation has to be supplemented by boundary-layers of dimensionless thickness $1/\sqrt{Re} = 1/\sqrt{Fr\, Ek}$ to fulfill the no-slip boundary conditions.

The boundary-layers suck and blow out fluid periodically and thus induce a secondary flow of order $1/\sqrt{Re}$. The interaction of the base flow with inviscid potential flow wave induce correction terms of the inviscid potential wave of order Fr and Fr^2. It can be shown that the term of order Fr of the growth rate vanishes. Thus, one has to inspect the terms of Fr^2 to determine the stability of the base flow.

We remark that the pressure variations in air due to an undulation of the interface water/air are of the order $Fr^2\sqrt{Ek}$ and thus smaller than the leading order terms which determine the stability limit.

4.1 Inviscid wave modes

By observing the large amplitude wave shown in Fig. 1b one may be reminded of well-known sloshing phenomena. Similar rotary waves can be excited by shaking a vertical cylindrical container. In a first stage, these waves can be described by potential flow theory. Thus, we summarize the potential flow theory of rotary waves, see Ibrahim [6].

For large Reynolds numbers and small wave amplitudes we can approximate the flow in the water by an inviscid potential flow, $\vec{u} = grad\ \varphi_0$, where φ_0 is the dimensionless flow potential. Combining the linearized kinematic and the dynamic boundary condition, we obtain the boundary condition at the top surface $z = 0$:

$$\phi_{0,tt} + \phi_{0,z} = 0. \tag{15}$$

A solution for the flow potential can be found by the product ansatz

$$\phi_0(r, z, \theta, t) = a(r)Z(z)\sin(n\theta - \omega_0 t), \tag{16}$$

$$h_0(r, \theta, t) = a(r)\omega_0 \cos(n\theta - \omega_0 t). \tag{17}$$

Inserting into the potential equation and separation of the variables yields

$$a(r) = J_n(\mu r), \quad Z(z) = \frac{\cosh \mu(z + h_w)}{\cosh h_w}, \tag{18}$$

where J_n is the Bessel function with index n and the constant μ is determined from the kinematic boundary condition $u(1) = 0$ at the container wall,

$$J_n'(\mu) = 0. \tag{19}$$

For every index $n \geq 1$, there is a sequence μ_{nk}, $k = 1,2,\ldots$ of zeros of the first derivative of J_n.
Inserting into the combined boundary condition (15) yields an equation for ω_0,

$$\omega_0^2 = \mu_{nk} \tanh \mu_{nk} h_w. \tag{20}$$

Thus, the dimensionless angular velocity is given by $\omega_{0/n}$ and the dimensionless frequency by $\omega_0/2\pi$. The wave form is given by

$$h(r, \theta, t) = J_n(\mu_{n.k} r)\cos(n\theta - \omega_0 t). \tag{21}$$

The first index n gives the number of maxima in the azimuthal direction, the second index k gives the number of local extrema in the radial direction. thus, the 1,1-mode

has one maximum in the azimuthal direction and one extremum at the boundary. The 1,2-mode has one local maximum at $r = 1.8141/5.3314 = 0.3403$.

4.2 Decay rate of the potential wave

The inviscid potential flow cannot satisfy the no-slip boundary conditions at the cylinder wall and at the bottom. Thus, near the wall and bottom time-periodic boundary-layers develop. These boundary-layers induce a secondary inviscid potential flow in the interior of the fluid domain. Since in this case, the boundary-layer equations are linear we can solve them analytically. The secondary potential flow together with the growth rate (damping) term $g_{1/2}$ of order $O(Re^{-\frac{1}{2}})$ can be determined analytically, see Ibrahim [6], p.163,

$$g_{1/2} = -\sqrt{\frac{\omega_0}{8}}\left(\frac{1+(n/\mu_{nk})^2}{1-(n/\mu_{nk})^2} - \frac{2\mu_{nk}h_w}{\sinh 2\mu_{nk}h_w}\right). \tag{22}$$

4.3 The stability limit

The equations for the expansion of the eigenfunctions and the growth rate g_2 can be found in Steinrueck et al. [12]. In the following, we evaluate g_2 numerically as a function of the Ekman number Ek for the two different shear stress distributions on the free surface.

In Fig. 4a the growth coefficient g_2 of different modes is shown for case 1. For the 1,1 mode and 1,2 mode the coefficient g_2 is positive for small Ekman numbers.
For $n,1$ modes with $n > 4$ there is in an interval of Ekman numbers, where g_2 is positive. However, for $Ek \to 0$ the growth coefficient g_2 becomes negative.

For the airflow in case 2, the situation is different. Here, g_2 stays negative for the modes 1,1, 1,2, 2,1, 3,1, 4,1. However, modes which are wavy at the circumference have intervals of Ekman numbers where g_2 is positive. The stability limit is given when $Fr^2 g_2$ exceeds $-Re^{-1/2}g_{1/2}$ or in other words g_2 exceeds $-Re^{3/2}Ek^2 g_2/g_{1/2}$.

These curves are indicated in Fig. 4b for three different Reynolds numbers. Thus, modes which are wavy at the circumference become unstable first.

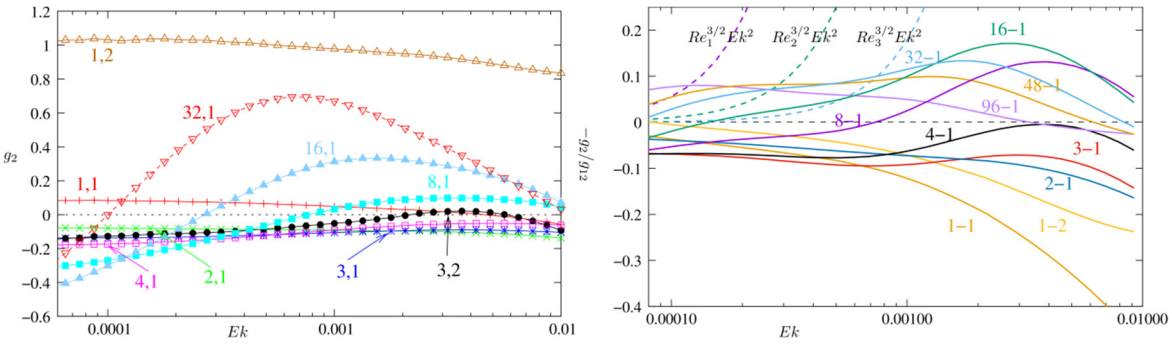

a) b)

Fig. 4. coefficient g_2 of growth rate in case 1 a) ratio of growth coefficients $-g_2/g_{1/2}$ (solid lines) and stability limit $Re^{3/2}\,Ek^2$ (dashed lines) for $Re_1 = 3\,10^5$, $Re_2 = \ 10^5$, $Re_3 = 3\,10^4$ for different waves modes for case 2 b)

5 Experimental results

For the experimental investigations, two test stands have been built. Both consist of a vertical cylinder and a disc rotating with the angular velocity Ω_A on the upper end. The characteristic data of both test stands is summarized
in table 2.

Test stand	Radius $\tilde{R}$	Height $\tilde{H}$	Disc speed $\tilde{\Omega}_A$	Re	$\tilde{t}_{damp} = \sqrt{Re\,\tilde{R}/\tilde{g}}$
	(m)	(m)	(rpm)	-	(s)
#1	0.1	0.8	$90 - 3000$	$0.99\,10^5$	31.8
#2	0.2	1.0	$200 - 100$	$2.9\,10^5$	75.6

Table 2: Characteristic data of the test stands

The smaller test stand is shown in Fig. 1a. The drive of the small test stand has 21 notches and the speed can be varied between 89.19 rpm and 2926 rpm. The speed of the disc of the large test stand can be controlled by a frequency converter.

The temporal evolution of the wave is recorded with a video camera, and the amplitude of the wave is determined using a millimetre grid on the cylinder. Moreover, the number of waves is counted at specific time instances.

For an air gap of $\tilde{h}_A = 31\,mm$ only small amplitudes for drive speeds less than $1382\,rpm$ have been observed. For $\tilde{\Omega}_A = 1523\,rpm$, the amplitude saturates at $25\,mm$. For $\tilde{\Omega}_A = 1769\,rpm$, shortly after the last data point the wave hits the disc. A similar behaviour was observed for $\tilde{h}_A = 35\,mm$ and $\tilde{h}_A = 37\,mm$.

In Fig. 5b, the growth of the amplitude for different water level disc distances $\tilde{h}_A$ is shown. For distances larger than $41\,mm$ the top speed of the disc $\tilde{\Omega}_A = 2927\,rpm$ was not sufficient to generate a large amplitude wave.

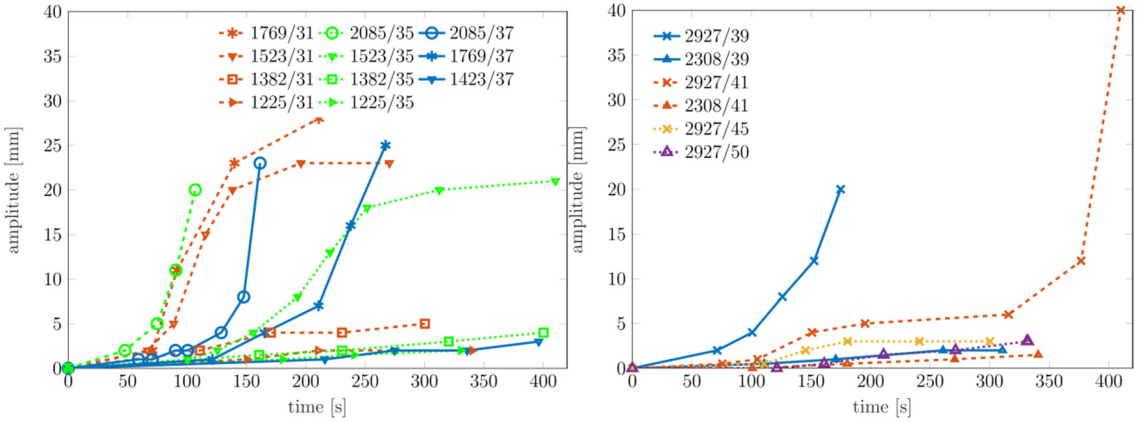

a) b)

Fig. 5. Amplitude of wave for a plain disc as a function of time for angular velocity and distance water disc $\tilde{\Omega}_A/\tilde{h}_A$

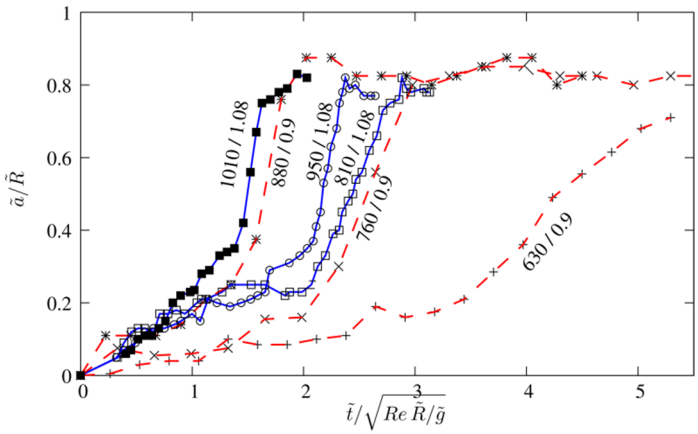

Fig. 6. Disc with profile: evolution of the wave amplitude. The numbers indicate the dimensionless disc speed (number of revolution per $\tilde{t}_{damp}$ and dimensionless distance of the water level to the disc.

A T-shaped profile has been mounted onto the rotating disc to enhance the rotating air flow. Thus, waves can be observed for a distance disc/water level $\tilde{h}_A = 150\,mm$. Experiments using a disc with a profile have been performed on both test stands. The evolution of the amplitude as a function of time is shown in dimensionless form in Fig. 6. We refer the time to the characteristic damping time

$$\tilde{t}_{damp} = \sqrt{Re\,\tilde{R}/\tilde{g}}$$

The speed of the driving disc is measured in revolutions per time interval of length $\tilde{t}_{damp}$. Experiments performed on test stand 1 are indicated with a solid line, experiments on test stand 2 with a dashed line.

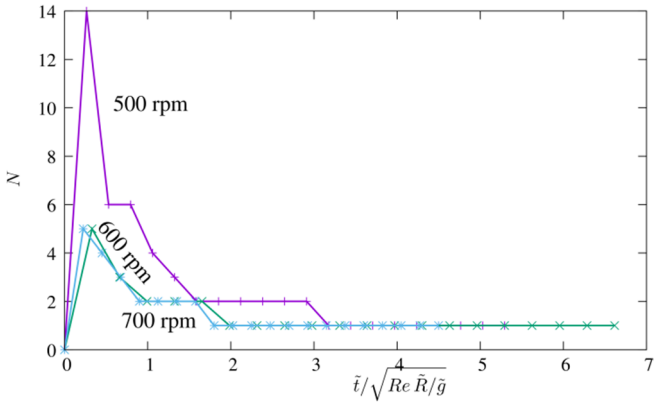

Fig. 7. Number of waves as a function of time

In Fig. 8 snapshots of the wave are taken are at certain time instances. The stopwatch in the pictures indicates the time elapsed from the start of the disc. At time $\tilde{t} = 0$ the fluid is at rest and the discs starts to rotate.

Immediately after the start of the disc motion, the surface waves with a short wavelength develop. They grow in amplitude and merge to waves with a longer wavelength. After 40s 6 wave crests can be identified at the circumference of the cylinder. After 120s the number of waves has been reduced to two. After 3 minutes an internal wave crest can be observed. After 4 min a superposition of waves with 2 two wave crests and a wave with only one wave crest can be identified. After 6 minutes the final rotary wave with only one wave crest has developed, see Fig. 7.

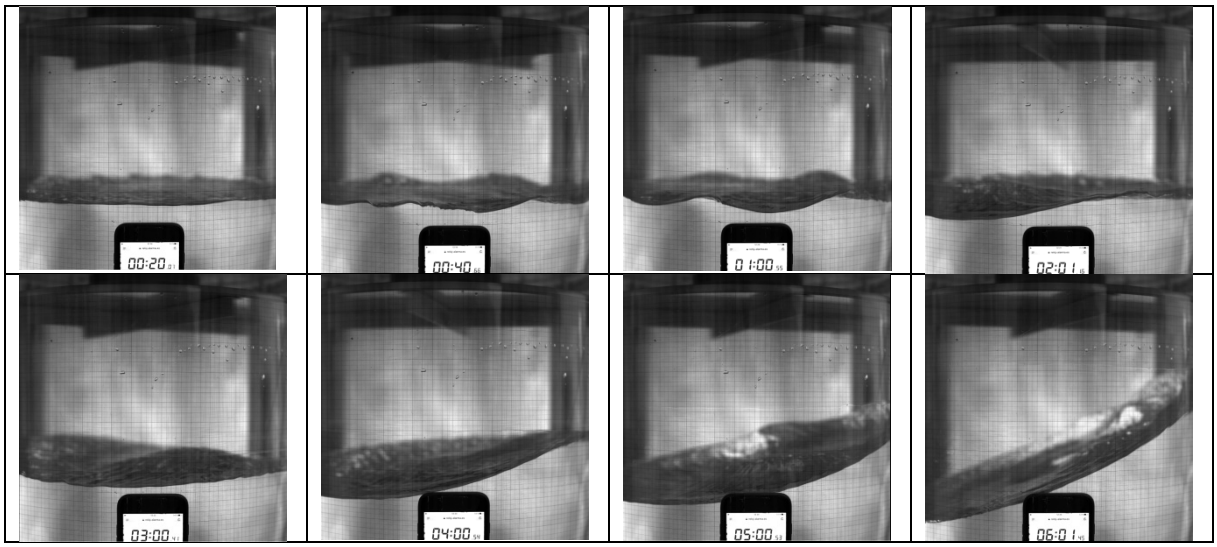

Fig. 8. Waveform as a function of time. Experiment performed on test stand 2. Stopwatch indicates time from starting at rest. $\widetilde{\Omega}_A = 500\,rpm$.

This behaviour is in accordance with the stability analysis which predicts an instability of a high wave number mode first.

6 Conclusions

We have discussed the stability of the base flow in a cylindrical container with respect to rotary waves excited by axis-symmetric shear stress on its surface. The stability of the modes depends crucially on the shear stress distribution at the free surface. Only for the unrealistic case of laminar air flow, the 1,1 mode is directly excited. In the other cases, the stability analysis predicts that wavy modes become unstable first.

Experiments confirm that wavy modes are excited first, and the large amplitude 1,1 mode forms only after some initial transient behaviour.

The methods presented in this study can be used to determine the onset of rotary waves when the air flow is known. However, it does not explain or predict the amplitude of the fully developed wave. An analysis of the large amplitude wave will be subject of further research.

References

[1] J. A. T. Bye and M. Ghantous. Observation of Kelvin-Helmholtz instability at the air-water interface in a circular domain. Physics of Fluids, 24, 2012.
[2] O. Cervavola, M. Fanelli, and B. Lazzaro. The behaviour of the free level below the runner of Francis turbines and pump-turbines in operation as synchronous condensers. In IAHR Symposium 1990, Tokyo.
[3] D. Dijkstra and G. J. F. van Heist. The flow between two finite rotating disks enclosed by a cylinder. J. Fluid Mech., 128, pp. 123-154, 1983.
[4] Y. Gelfgat, P.Z. Bar-Yoseph, and A. Solan. Stability of confined swirling flow with and without vortex breakdown. J. Fluid Mech., 311 pp. 1-36, 1996.
[5] M. Ghantous and J. A. T. Bye. Interfacial instability of coupled-rotating inviscid fluids. J. Fluid Mech.,730, pp. 343-363, 2013.
[6] R. Ibrahim. Liquid Sloshing Dynamics, Theory and Applications. Cambridge Univ. Press, 2005.
[7] J. W. Miles. On the generation of surface water waves by shear flow. J. Fluid Mech., 3, pp. 185-204, 1957.
[8] S. Sajjadi. Growth of Stokes waves induced by wind on a viscous liquid of infinite depth. Advances and Applications in Fluid Dynamics, 19, 2016.
[9] K. Schlichting and H. Gersten. Boundary-layer theory, Springer, 8th edition 2000.
[10] H. Steinrück and L. Gusner. The excitation mechanism of a shear stress-induced rotary wave. PAMM 16, pp. 613-614, 2016.
[11] H. Steinrück and A. Maly. Experimental and asymptotic investigation of a rotary wave in a cylindrical container. PAMM 17, pp. 667-668, 2017.
[12] H. Steinrück, A. Maly and G. Glanz. A rotary wave in phase condenser mode. Conference on Modelling Fluid Flow (CMFF'18), Budapest 2018.
[13] H. Tanaka, K. Matsumoto, and K. Yamamoto. Sloshing motion of the depressed water in the draft tube in dewatered operation of high head pump turbines. In XVII IAHR SYMPOSIUM, pp. 121-130, 1994.
[14] E. Vagnoni, A. Faverel, L. Andolfatto, and F. Avellan. Experimental investigation of the sloshing motion of the water free surface in the draft tube of a Francis turbine operating in synchronous condenser mode. Experiments in Fluids 59:95, 2018.

Author(s)

Dr. Herbert STEINRÜCK,
Vienna University of Technology
Institute for Fluid Mechanics and Heat Transfer
Getreidemarkt 9/322, A-1060 Vienna, AUSTRIA
Phone: +43-1-58801-32231 FAX +43-1-58801-32299,
E-mail: herbert.steinrueck@tuwien.ac.at

Herbert Steinrück received his PhD in Applied Mathematics at the TU Wien in 1985 and the venia docendi in Applied Mathematics in 1991. He joined the Institute for Fluid Mechanics and Heat Transfer at the TU Wien in 1992 and has currently the position of an associate Professor.

Dipl.-Ing. Anton MALY,
Vienna University of Technology
Institute for Energy Systems and Thermodynamics
Getreidemarkt 9/302, A-1060 Vienna, AUSTRIA
Phone: +43-1-58801-302413 FAX +43-1-58801-302399,
E-mail: anton.maly@tuwien.ac.at

Anton Maly graduated in Mechanical Engineering at the Vienna University of Technology in 2015. Currently he is working as project assistant at the Institute for Energy Systems and Thermodynamics (IET) at the TU Wien.